

On the accuracy of RANS simulations with DNS data.

Svetlana V. Poroseva^{1),a)}, Juan D. Colmenares F.¹⁾, and Scott M. Murman²⁾

¹*Mechanical Engineering Department, University of New Mexico, Albuquerque, NM, 87131, U.S.A.*

²*NASA Ames Research Center, Moffett Field, CA 94035, U.S.A.*

ABSTRACT

Simulation results conducted for incompressible planar wall-bounded turbulent flows with the Reynolds-Averaged Navier-Stokes (RANS) equations with no modeling involved are presented. Instead, all terms but the molecular diffusion are represented by the data from direct numerical simulation (DNS). In simulations, the transport equations for velocity moments through the second order (and the fourth order where the data are available) are solved in a zero-pressure gradient boundary layer over a flat plate and in a fully-developed channel flow in a wide range of Reynolds numbers using DNS data from Sillero et al. (2013), Lee & Moser (2015), and Jeyapaul et al. (2015). The results obtained demonstrate that DNS data are the significant and dominant source of uncertainty in such simulations (hereafter, RANS-DNS simulations). Effects of the Reynolds number, flow geometry, and the velocity moment order as well as an uncertainty quantification technique used to collect the DNS data on the results of RANS-DNS simulations are analyzed. New criteria for uncertainty quantification in statistical data collected from DNS are proposed to guarantee the data accuracy sufficient for their use in RANS equations and for the turbulence model validation.

^{a)} poroseva@unm.edu

I. INTRODUCTION

Despite their ubiquity, it is surprisingly difficult to quantitatively characterize the quality of direct numerical simulations (DNS) of turbulent flows. Efforts are typically directed towards minimizing errors in simulations by utilizing the highest resolution in time and space accessible on the latest computational hardware. Statistical errors in data collected from DNS are controlled by estimating the statistical convergence of DNS results using heuristics, such as monitoring the balance errors in the transport equations for second-order velocity moments.

This traditional approach to DNS data error analysis, while providing confidence that the results obtained meet reasonable standards of accuracy, does not answer the most imperative questions, that is, how accurate is a single simulation in the given flow and how much uncertainty remains in statistics collected from DNS. As a result, only subjective comparison of the quality of different DNS databases can be made. This shortcoming is problematic going forward, as DNS of more complex configurations and flows are expected, where the legacy rules of thumb developed for pseudo-spectral methods may no longer be relevant.

The total uncertainty in DNS data comprises errors and uncertainties from various sources, such as discretization error, statistical sampling error, and the discretization error in the statistical sampling itself¹. Ideally, one would like these errors to all be of the same order of magnitude, else extra work is being done in some arena for no benefit. To the authors' knowledge, analyzing the coupled sources of error has not been rigorously examined beyond model problems. Starting with the work of Orszag², significant attention has been given to discretization and aliasing errors in DNS, however the analysis of errors due to the finite statistical sample sizes available in DNS is less mature.

A standard procedure for evaluating the total uncertainty in statistical data collected from DNS was first used in Mansour et al.³ and possibly in Rogallo⁴. Neither of the studies directly mentions the procedure, but there is a consensus about the origin of the approach. In the procedure, uncertainty in the collected Reynolds stresses is linked to the budget balance errors. The errors vary for different Reynolds stresses depending upon the spatial coordinates and the averaging time. Uncertainty in the data is reduced by increasing the number of flow realizations and demonstrated by comparing the orders of magnitude of the budget balance errors to the leading (largest) terms in the governing equations. The acceptable level of uncertainty in the collected Reynolds stresses is determined by a subjective judgment rather than by a rigorous procedure and is strongly influenced by the cost of computations.

In Hoyas & Jiménez⁵, the above procedure for evaluating the order of magnitude of the budget balance errors is complemented with an estimate of the statistical errors. The statistical error estimate is based on the standard deviation of the variables, which are individual terms in the Reynolds stresses budgets. A procedure is proposed to represent each of the two estimates (budget balance errors and statistical errors) by a single number for the given Reynolds stress. The maximum of the two numbers determines the total uncertainty in the Reynolds stress calculation. Although a step forward, the procedure is complex to implement, with the results dependent on a specification of a non-unique parameter. The results computed in Hoyas & Jiménez⁵ for a zero-pressure gradient boundary layer (ZPGBL) adhere to the common perception that the contribution of numerical errors in statistics collected from DNS is secondary in comparison with the statistical errors due to the limited averaging time (finite number of decorrelated flow realizations).

Recent uncertainty analysis of DNS data by Oliver et al.⁶ using a Bayesian extension of Richardson extrapolation⁷ partially confirmed the results of Hoyas & Jiménez⁵. That is, they

demonstrated that large contributions from the discretization errors could not be completely ruled out for all collected statistics. On the other hand, the uncertainty model proposed in Oliver et al.⁶ may also affect the results, as numerous assumptions and simplifications are made during its formulation and application. The procedure is limited to the numerical schemes and flow geometries used in Oliver et al.⁶.

In the current work, a new approach is demonstrated to examine the uncertainty in statistical data collected from DNS. The approach utilizes self-consistency of the Reynolds-averaged Navier-Stokes (RANS) equations, wherein the computed statistics from DNS themselves are used to solve the equations, and their solutions are compared back with the DNS data for velocity moments. Hereafter, such computations are called RANS-DNS simulations. The procedure is amenable to any flow geometry and straightforward to implement.

The use of RANS-DNS simulations has further implications for the development and evaluation of RANS models. Since DNS data are the most accurate computational representation of the individual terms in RANS equations, it is reasonable to assume that the use of DNS data instead of RANS models for unknown terms will lead to the most accurate computational solutions of RANS equations. When RANS-DNS simulations do not produce accurate results, physics-based RANS models, which have the objective of replicating the details of the Reynolds stress behavior, cannot be expected to perform any better.

In the current paper, DNS data collected for two planar wall-bounded flows – a fully-developed turbulent channel flow^{8,9} and a ZPGBL over a flat plate¹⁰ – are used to demonstrate the RANS-DNS approach. In the channel flow simulations, statistics used are obtained at four Reynolds numbers: $Re_\tau = 180$, 550, and 5200 in Lee & Moser⁸ and $Re_\tau = 392$ in Jeyapaul et al.⁹ (Re_τ is based on the friction velocity and the channel half-height). In the boundary layer, DNS data from

Sillero et al.¹⁰ are available at six locations along the flat plate in the range of Re_θ from 4000 to 6500 with the increment of 500 (Re_θ is based on the free stream velocity and the boundary layer momentum thickness θ). Note that the DNS databases from Lee & Moser⁸ and Sillero et al.¹⁰ use the statistical guidelines developed by Oliver et al.⁶ in the case of a channel flow, and Hoyas & Jiménez⁵ in the case of a ZPGBL, respectively, providing a comparison of these statistical measures against the current RANS-DNS approach. The standard balance error procedure described above is used in Jeyapaul et al.⁹.

II. RANS-DNS SIMULATIONS

In RANS-DNS simulations, the exact RANS equations are solved, with no modeling involved. All budget terms except for the molecular diffusion are substituted with the data collected from DNS for these terms. In such a formulation, all equations are uncoupled, that is, there is no interdependency of their solutions. The solutions are compared with the DNS data for the corresponding velocity moments. The discrepancy between the RANS-DNS simulation solution and the DNS profile of the corresponding velocity moment serves as an indicator of the solution inaccuracy.

The following requirements determine the molecular diffusion as the only term left for solving in the RANS equations. The simulation framework should be applicable to various flows. From the terms containing unknown velocity moments in the RANS equations – molecular diffusion, turbulence production, and convection – the convective terms disappear in fully-developed turbulent flows, and therefore, cannot be left as the only unknown in the equations. The other requirement to RANS-DNS simulations is the use of already existing solvers for RANS

simulations. Leaving the turbulence production as unknown would transform the equations from differential to algebraic and require different solvers for their solution.

There are two major contributors to inaccuracy in the RANS-DNS simulation solutions: a numerical procedure used to solve the RANS equations and inaccuracies in DNS data. Their interaction may also be a factor. As shown in the *Results and Discussion* section, inaccuracies in the DNS data dominate the RANS-DNS simulation results, so that they are insensitive to improvements in the numerical procedure. This makes the proposed simulations suitable for uncertainty quantification specifically in DNS data.

In the paper, the RANS equations are solved in a fully-developed turbulent channel flow and in a ZPGBL. In the channel flow, transport equations for the mean flow velocity and velocity moments through the fourth order are used:

$$0 = D_{ij}^M + D_{ij}^T + P_{ij} + \Pi_{ij} - \varepsilon_{ij}, \quad (1)$$

$$0 = D_{ijk}^M + D_{ijk}^T + P_{ijk} + P_{ijk}^{(T)} + \Pi_{ijk} - \varepsilon_{ijk}, \quad (2)$$

$$0 = D_{ijkl}^M + D_{ijkl}^T + P_{ijkl} + P_{ijkl}^{(T)} + \Pi_{ijkl} - \varepsilon_{ijkl}. \quad (3)$$

In a ZPGBL, the equations for velocity moments of the second order (Reynolds stresses) are computed using:

$$C_{ij} = D_{ij}^M + D_{ij}^T + P_{ij} + \Pi_{ij} - \varepsilon_{ij}. \quad (4)$$

In equations (1)-(4), tensors P , P^T , Π , ε , D^T , D^M , and C are the production by strain (associated with the mean velocity gradients), production by turbulence (associated with the Reynolds stress gradients), velocity/pressure-gradient correlations, dissipation, turbulent diffusion, molecular diffusion, and convection, respectively.

Exact expressions used in simulations for each term in equations (1)-(4) are obtained from equation (A2) given in the Appendix. Equation (A2) represents RANS equations in planar incompressible turbulent flows in the general form. In the channel flow, equation (A2) (along with equation (A1) for the mean flow velocity) is simplified under the assumption of a statistically stationary fully-developed turbulent flow, while in a ZPGBL, a statistically stationary spatially developing flow is assumed.

Jeyapaul et al.⁹ provide DNS statistics through the fourth-order moments in a channel flow, hence the full set of equations (1)-(3) are solved for these moments. The datasets of Lee & Moser⁸ and Sillero et al.¹⁰ contain statistics through the second order, hence equations (1) and (4) are used, respectively. The mean flow velocity is computed only in the channel flow. In a ZPGBL, solutions for the mean flow velocities could not be obtained. We think that this is because the DNS data necessary for computing these flow parameters are only available at three locations along a flat plate to compare with six locations where the data for the Reynolds stresses are provided.

The cubic spline function is used when interpolation of the DNS data is required in this study. Other interpolation schemes and additional smoothing procedures were tested, and did not change the simulation results.

III. NUMERICAL PROCEDURE

A. Channel flow simulations

Two solvers are used in the channel flow simulations with DNS data from Jeyapaul et al.⁹ in order to verify that the computed results are independent of implementation: an in-house second-order-accurate code for fully-developed axisymmetric flows, and the open-source OpenFOAM software¹¹. Simulations were conducted to analyze the effects of discretization errors and a numerical scheme in the RANS-DNS simulations.

In the in-house code, the control volume technique¹² is implemented with a pseudo-time marching scheme with time step of 0.1s to solve parabolic equations. The grid is non-uniform in the direction normal to the channel wall with the total number of nodes in this direction being 100 (a 97-node grid was used in DNS⁹). This grid resolution was found to be sufficient for obtaining grid-independent results. At the channel wall, a no-slip boundary condition is applied to all flow parameters for which the transport equations are solved. At the channel axis,

$$\frac{\partial U}{\partial y} = \frac{\partial \langle u_\alpha u_\alpha \rangle}{\partial y} = \langle uv \rangle = 0 ,$$

is specified, where $\alpha = x, y, z$, (no summation over α). DNS profiles interpolated to the grid nodes are used as initial conditions to accelerate the results convergence.

In simulations with OpenFOAM, the *simpleFoam* application from the OpenFOAM 2.3.0 library¹¹ is used to solve the Reynolds stress transport equations with a Preconditioned Bi-Conjugate Gradient solver (*PBiCG*) and a Diagonal Incomplete LU (*DILU*) preconditioner. Table 1 provides a list of numerical schemes used to discretize the equations.

Table 1. Numerical schemes as specified in the OpenFOAM *fvSchemes* file.

Calculation	Keyword	Scheme
Gradient	<i>gradSchemes</i>	<i>Gauss linear</i>
Convection	<i>divSchemes</i>	<i>bounded Gauss linear</i>
Laplacian	<i>laplacianSchemes</i>	<i>Gauss linear corrected</i>
Time derivative	<i>timeScheme</i>	<i>steadyState</i>

The pressure-gradient source term in the mean flow velocity equation is added by specifying the *pressureGradientExplicitSource* option in the *momentumSource* dictionary, placed in the *fvOptions* OpenFOAM file inside the *system* directory of a case under consideration. The applied pressure gradient is chosen to match the DNS results.

The computational domain dimensions are $L_x \times L_y \times L_z = 0.1 \times 2 \times 0.1$, in the unit length h , which is the channel half-width. Although the flow is fully-developed, three-dimensional grids are required by OpenFOAM. The grid size is $N_x \times N_y \times N_z = 2 \times 193 \times 2$ nodes. The number of grid nodes and the distribution in the wall-normal direction over the channel half-width are identical to that of the DNS data points in this direction. Initial values at the cell centers are interpolated from the DNS profiles available at the nodes⁹.

Periodic (*cyclic*) boundary conditions are applied at the faces normal to the streamwise direction. Faces normal to the spanwise direction are defined as *empty*, which is a special type of boundary conditions used in OpenFOAM for two-dimensional problems. The remaining faces are defined as the type *wall*, where no-slip boundary conditions are applied to all flow parameters for which the equations are solved.

RANS-DNS simulations conducted with the two solvers using DNS data from Jeyapaul et al.⁹ produced similar results demonstrating a secondary effect of a numerical procedure on the results of RANS-DNS simulations. Therefore, the channel flow simulations with DNS data from Lee &

Moser⁸ and the ZPGBL simulations with the data from Sillero et al.¹⁰ were conducted with OpenFOAM only.

For RANS-DNS simulations with the data from Lee & Moser⁸, different grids were generated to match the distribution of grid nodes in DNS:

Table 2. The grid resolution used in RANS-DNS simulations with the data from Lee & Moser⁸.

Re_τ	$N_x \times N_y \times N_z$
180	$2 \times 191 \times 2$
550	$2 \times 383 \times 2$
5200	$2 \times 1535 \times 2$

Notice that DNS data⁸ are not available at the channel axis ($y/h = 1$). Therefore, data from the DNS grid point closest to the channel half-width are used to calculate values of the parameters at the center of the cell adjacent to the channel half-width. The bulk mean flow velocity in these simulations corresponds to the DNS value of 1 m/s. Other details of the numerical procedure are the same as described above for the RANS-DNS simulations with the data from Jeyapaul et al.⁹.

B. ZPGBL simulations

Dimensions of the computational domain used in the ZPGBL simulations are: $L_x \times L_y \times L_z = 494.24 \times 39.55 \times 1$ in the unit length. The L_x size is chosen to match the range of Reynolds numbers for which the DNS data¹⁰ are available: $4000 \leq Re_\theta \leq 6500$. The length L_y corresponds to the maximum location away from the wall at which the DNS data are available.

The DNS data¹⁰ are available at six locations corresponding to $Re_\theta = 4000, 4500, 5000, 5500, 6000, \text{ and } 6500$. The DNS data are interpolated on the grid with the uniform node distribution in the streamwise direction. It was found that 100 cells are enough to correctly capture the gradients

in this direction in simulations. The number of nodes in the normal-to-the-wall direction corresponds to that from DNS. The node locations are determined as the average of the y positions obtained from the different DNS profiles, which slightly vary at different Reynolds numbers. The final grid size is $N_x \times N_y \times N_z = 101 \times 535 \times 2$.

The boundary conditions assigned at the top of the computational domain are interpolated from the DNS data. The no-slip boundary condition is assigned at the wall for the Reynolds stresses. The data at $Re_\theta = 4000$ and 6500 are used as the inlet and exit boundary conditions. Other details of the numerical procedure relevant to the ZPGBL simulations are the same as described above for the channel flow simulations.

IV. RESULTS AND DISCUSSION

A. Channel flow simulations with DNS data from Jeyapaul et al.⁹

In Jeyapaul et al.⁹, DNS data are provided for velocity moments through the fourth order and their budget terms at $Re_\tau = 392$, which makes this database unique and of interest for the current study.

The results of RANS-DNS simulations conducted using OpenFOAM with the DNS budget terms from Jeyapaul et al.⁹ are shown in Figs. 1-3 in comparison with the DNS profiles for the mean flow velocity and velocity moments from the same database. The DNS profiles in Figs. 1-3 and the following ones are marked by symbols; lines correspond to the results from RANS-DNS simulations. In particular, the calculated mean flow velocities are shown by the dashed lines; the solutions of equations (1)-(3) are shown by the dashed lines with and without dots.

A strong disagreement between the calculated velocity moments and their corresponding DNS profiles is observed for all considered velocity moments in the figures. The mean flow velocity

calculated from RANS-DNS simulations also deviates from its DNS profile, although to a lesser degree than the velocity moments.

B. Channel flow simulations with DNS data from Lee & Moser⁸

DNS statistics from Jeyapaul et al.⁹ were collected using the standard approach³ to evaluating the DNS data accuracy. In Lee & Moser⁸, the procedure proposed by Oliver et al.⁶ was used for the same purposes as a more rigorous alternative to the standard approach³. Further, a finer grid was used in Lee & Moser⁸ reducing the discretization error in DNS: 192 vs. 97 nodes for a half channel width, with the grid spacing at the wall in the y -direction being $\Delta y^+ = 0.019$ vs. 0.1, where $y^+ = yu_\tau/\nu$. The balance errors reported in Lee & Moser⁸ are at least the order of magnitude less than those in Jeyapaul et al.⁹. Only the mean flow velocity and Reynolds stresses budgets are available in Lee & Moser⁸. However, the data accuracy and availability at several Reynolds numbers allow for the examination of trends in the current study.

Here, the results of RANS-DNS simulations conducted with the DNS budget terms from Lee & Moser⁸ at three Reynolds numbers: $Re_\tau = 180, 550, \text{ and } 5200$, are presented. Equation (1) is used to calculate the Reynolds stresses.

The results of RANS-DNS simulations are shown in Figs. 4-7 by lines. As seen from the figures, the trends are similar to those obtained with the data from Jeyapaul et al.⁹. That is, the Reynolds stresses calculated from equation (1) (non-solid lines in Figs. 4-6) deviate from their DNS profiles even at the lowest Reynolds number, $Re_\tau = 180$.

Solutions of equation (1) obtained from RANS-DNS simulations are sensitive to the Reynolds number: the higher Reynolds number, the farther solutions deviate from the DNS profiles of the Reynolds stresses.

Inaccuracies in the DNS budgets impact to a lesser degree the mean flow velocity calculated from RANS-DNS simulations (Fig. 7). At $Re_\tau = 180$, the result from RANS-DNS simulations is in agreement with the mean flow velocity profile from DNS. At higher Reynolds number, $Re_\tau = 550$, a small discrepancy between the calculated and DNS profiles becomes apparent. At the highest Reynolds number, $Re_\tau = 5200$, a difference between the mean flow velocity profiles from RANS-DNS simulations and DNS is pronounced.

C. Boundary layer simulations with DNS data from Sillero et al.¹⁰

DNS data in Lee & Moser⁸ and Jeyapaul et al.⁹ were obtained in the same flow geometry, a planar fully-developed turbulent channel flow. To verify whether the observations made from the results of RANS-DNS simulations are general, rather than being specific for the channel flow, RANS-DNS simulations were also conducted in another wall-bounded flow, a ZPGBL, with DNS data from Sillero et al.¹⁰ being used in the simulations. The DNS data¹⁰ were collected using the procedure proposed in Hoyas & Jiménez⁵ for evaluating the data accuracy.

The Reynolds stresses budgets from Sillero et al.¹⁰ are available at six locations along the flat plate in the range of Re_θ from 4000 to 6500 with the increment of 500. Less data are available for the mean flow velocity budgets and in the locations different from those where the Reynolds stresses budgets are provided¹⁰. As a result, solutions for the mean flow velocities could not be obtained from the RANS-DNS simulations in this flow. Therefore, only results for the Reynolds stresses are discussed in what follows. Solutions for the Reynolds stresses were obtained from equation (4) using OpenFOAM.

In the conducted RANS-DNS simulations, DNS data at $Re_\theta = 4000$ and 6500 were used as the boundary conditions. Therefore, comparison of the results of RANS-DNS simulations with the

Reynolds stresses from DNS was made at four locations along the flat plate corresponding to $Re_\theta = 4500, 5000, 5500, 6000$. Because comparison led to similar conclusions at the four locations, the results are presented at only two locations, $Re_\theta = 4500$ and 6000 (Figs. 8 and 9), for brevity. In the figures, DNS profiles are shown by symbols; non-solid lines are the RANS-DNS simulation solutions of equation (4) (Figs. 8a, 8b, 9a, and 9b). The figures demonstrate the same behavior observed in the channel flow, that is, the results from RANS-DNS simulations deviate from the corresponding DNS profiles of the Reynolds stresses. The dependence of this phenomenon on the Reynolds number is also observed.

D. Uncertainty analysis in RANS-DNS simulations

Possible causes of the discrepancy between the results from RANS-DNS simulations and the DNS data are uncertainties associated with the numerical procedure used in RANS simulations and inaccuracies present in the DNS data. Their interaction may also be a factor. A thorough investigation has been conducted to evaluate the contribution of the RANS numerical procedure in the results shown in Figs. 1-9, which included conducting simulations in a channel flow with two different solvers using different grid refinements and different interpolation schemes.

Profiles of the Reynolds stresses obtained from RANS-DNS simulations with the two different solvers described in *Section III* are shown in Fig. 10a. DNS data from Jeyapaul et al.⁹ were used in these simulations. In the figure, solid lines are solutions from simulations with OpenFOAM and dashed lines are from simulations with the in-house code. The results from the two separate solvers are virtually indistinguishable.

The Reynolds stresses obtained from RANS-DNS simulations with different interpolations schemes are compared in Fig. 10b. The simulations were conducted with the DNS data from Lee

& Moser⁸ using OpenFOAM. Three interpolation schemes were used in the simulations: cubic splines, quadratic splines, and Radial Basic Functions¹³ (RBF). In the figure, results obtained with the different schemes are shown by solid (cubic splines), dashed (quadratic splines), and dash-dotted lines (RBF) at $Re_\tau = 550$. As with the variation of numerical method, there is essentially no sensitivity in the computed results to the type of accuracy of the interpolation scheme chosen.

Figure 10 indicates that the results of RANS-DNS simulations are hardly affected by variations in the RANS numerical procedure. This leaves inaccuracies in the DNS data as the only potential cause of uncertainty in the RANS-DNS simulation results.

To examine this issue, a numerical test is conducted whereby the RANS-DNS simulations are performed with the DNS data of Lee & Moser⁸ interpolated on the coarser grid used by Jeyapaul et al.⁹ Recall from the previous discussion that the RANS-DNS simulations with the DNS data from Jeyapaul et al.⁹ do not maintain consistency, whereas Lee & Moser's finer resolution data do produce the mean-flow profiles consistent with the DNS profiles at smaller Reynolds numbers. Figure 11a demonstrates that Lee & Moser's data also maintains consistency on the grid from Jeyapaul et al.⁹ with coarser resolution. In fact, this is demonstrated more strongly by coarsening the grid even further by removing every second grid point in the grid from Jeyapaul et al.⁹. The RANS-DNS simulation results with Lee & Moser's data at $Re_\tau = 550$ are still consistent with the DNS profile of the mean flow velocity. Variations in the grid resolution have similar effect of the Reynolds stresses calculated from the RANS-DNS simulations as shown in Fig. 11b at $Re_\tau = 550$. Overall, the results obtained indicate that Lee & Moser's data is inherently different than the data of Jeyapaul et al., either due to resolution, post-processing methodology, or other reasons.

Figures 10 and 11 show that the results of RANS-DNS simulations are hardly affected by variations in the RANS numerical procedure. This leaves inaccuracies in the DNS data as the only potential cause of uncertainty in the RANS-DNS simulation results.

To confirm this conclusion, RANS-DNS simulations were conducted with the RANS equations modified in the following manner:

$$0 = D_{ij}^M + D_{ij}^T + P_{ij} + \Pi_{ij} - \varepsilon_{ij} - \mathbf{Err}_{ij}, \quad (5)$$

$$0 = D_{ijk}^M + D_{ijk}^T + P_{ijk} + P_{ijk}^{(T)} + \Pi_{ijk} - \varepsilon_{ijk} - \mathbf{Err}_{ijk}, \quad (6)$$

$$0 = D_{ijkl}^M + D_{ijkl}^T + P_{ijkl} + P_{ijkl}^{(T)} + \Pi_{ijkl} - \varepsilon_{ijkl} - \mathbf{Err}_{ijkl}, \quad (7)$$

where the added source terms **Err** describe errors in the DNS budgets.

In most of the equations, the **Err** term is the balance errors from the DNS budget for the corresponding velocity moment. However, budgets for some velocity moments include non-zero values for the terms that should theoretically be zero in planar flows, such as, for example, the production term P_{zz} in the balance of $\langle w^2 \rangle$. (Hereafter, such terms are called “zero-value” terms.) Non-zero values of such terms result from insufficient sample size in the DNS. Their effect on the results of RANS-DNS simulations was initially studied in Poroseva et al.¹⁴ using DNS data of Jeyapaul et al.⁹ for the Reynolds stresses and found to be non-negligible. In the current study, a non-negligible effect of “zero-value” terms on the results of RANS-DNS simulations was also confirmed for higher-order velocity moments. When a “zero-value” term appears in the DNS

budget of a velocity moment, the *Err*-term in the corresponding equation of (5)-(7) is a sum of the budget balance errors and “zero-value” terms.

Balance errors are not available for the mean flow velocity budgets. Therefore, simulations similar to those with equations (5)-(7) for the velocity moments were not conducted for this flow parameter in the current study.

The solutions of equations (5)-(7) in a channel flow are shown in Figs. 1-6 by solid lines. The calculated velocity moments of all considered orders and at all considered Reynolds numbers are now in excellent agreement with their DNS profiles. That is indeed, the DNS data are the dominant uncertainty source in RANS-DNS simulations. The results also suggest that the observed effect of the Reynolds number on the solutions of equation (1) is due to inaccuracies in the DNS budgets.

In a ZPGBL, the computed results (solid lines in Figs. 8c, 8d, 9c and 9d) also become consistent with the DNS data if one modifies equation (4) in a manner similar to the modifications applied to equations (1)-(3):

$$C_{ij} = D_{ij}^M + D_{ij}^T + P_{ij} + \Pi_{ij} - \varepsilon_{ij} - Err_{ij}. \quad (8)$$

To summarize the results shown in Figs. 1-11, they suggest that the errors in DNS budgets are significant and the primary source of uncertainty in the results of RANS-DNS simulations in both considered flow geometries. Only at the lowest Reynolds number in the channel flow ($Re_\tau = 180$) these errors can be considered negligible in simulations of the mean flow velocity and the smallest Reynolds stresses, $\langle v^2 \rangle$ and $\langle uv \rangle$. Since statistics in the considered DNS datasets⁸⁻¹⁰ were collected to ensure that the balance errors are small, the RANS-DNS simulation results imply that the criteria used in those studies do not guarantee that the errors are small enough.

E. The analysis of DNS balance errors

As demonstrated in *Section D*, the DNS data are the dominant uncertainty source in RANS-DNS simulations and uncertainties associated with the RANS numerical procedure have negligible effect on the simulation results. This makes RANS-DNS simulations a plausible framework for the analysis of uncertainty in statistics collected from DNS. Below, we investigate the velocity moment budgets⁸⁻¹⁰ with the purpose of better understanding the requirements for the balance errors to be considered small enough for their use of DNS data in RANS-DNS simulations.

Let us first compare the balance errors in different datasets^{8,9} in the fully-developed channel flow at the close Reynolds numbers: $Re_\tau = 392$ and 550 . These two datasets were collected using different procedures^{3,6} for uncertainty quantification in DNS statistics. The errors in both datasets appear small, less than 0.1% of the Reynolds stress values, as shown in Fig. 12 for the smallest of Reynolds stress components, $\langle v^2 \rangle$. However, as demonstrated in Figs. 1 and 5, this error level is not small enough when the data are used in RANS-DNS simulations.

Comparison of the balance errors with the velocity moment values is still informative when comparing the accuracy of different datasets. Figures 1 and 5 show that the RANS-DNS simulation results obtained with the DNS data from Lee & Moser⁸ are more accurate than those obtained with the data from Jeyapaul et al.⁹ at a lower Reynolds number. This is in agreement with the results in Fig. 12a for $\langle v^2 \rangle$ showing that the normalized balance errors from Lee & Moser⁸ are at least the order of magnitude less than those reported in Jeyapaul et al.⁹ Similar observations were made for all Reynolds stresses.

Although available data allows for comparison of the accuracy of the two DNS datasets^{8,9}, they do not provide enough information for evaluating a contribution of the uncertainty quantification procedure into the data accuracy. In addition to differences in the procedures used, different grids

were utilized in the two studies, among other factors. That is, the grid with 192 nodes in a half channel width was used in Lee & Moser⁸ to compare with 97 nodes used in Jeyapaul et al.⁹. The grid spacing at the wall in the normal-to-the-wall direction was $\Delta y^+ = 0.019$ and 0.1 in Lee & Moser⁸ and Jeyapaul et al.⁹, respectively, where $y^+ = yu_\tau/\nu$.

Comparison of the balance errors to the velocity moment values may also be misleading. For example, the RANS-DNS simulation results in the channel flow (Figs. 4-7) obtained with the DNS data from the same dataset⁸ at different Reynolds numbers unambiguously demonstrate degradation of the data accuracy with increasing the Reynolds number. This tendency is also apparent in a ZPGBL (Figs. 8-9). However, no such loss in the DNS data accuracy is detected when one monitors the balance errors normalized by the Reynolds stress values. Moreover, the errors in the channel flow seem to reduce with the increase in the Reynolds number. This is illustrated in Figs. 13 and 14 for the smallest Reynolds stress $\langle v^2 \rangle$, but such results were obtained for all Reynolds stresses.

Similarly, if one compares the balance errors with the leading terms in a velocity moment budget, no growth of errors with increasing the Reynolds number is observed. With such normalization, the balance errors instead tend to collapse to the same level at different Reynolds numbers. Figs. 15 and 16 present the balance errors in the budgets of the largest and smallest Reynolds stresses – $\langle u^2 \rangle$ and $\langle v^2 \rangle$ – in the channel flow and in a ZPGBL, respectively. In the $\langle v^2 \rangle$ -budgets, the leading terms are velocity/pressure-gradient correlations and viscous dissipation, and in the $\langle u^2 \rangle$ -budgets, the production and viscous dissipation lead. Although the results in the figures are shown for the balance errors in comparison with Π_{yy} and P_{xx} , similar observations are made when compared against the dissipation terms. Also, similar results are obtained for the two other Reynolds stresses not shown here.

It is interesting to note that the error level in such normalization is the same for different Reynolds stresses, that is, less than 1% in Lee & Moser⁸ in the most of the channel flow except for the area close to the channel axis, and somewhat higher, less than 10% in Sillero et al.¹⁰ The same level of balance errors as in Sillero et al.¹⁰ is obtained with the data from Jeyapaul et al.⁹ (Fig. 12b).

When comparing the accuracy of data in different DNS datasets for the same flow geometry, the conclusion does not change whether the balance errors are normalized by the leading terms in the Reynolds stresses budgets or by the Reynolds stress values. That is, the data in Lee & Moser⁸ are about one order of magnitude more accurate than the data in Jeyapaul et al.⁹ as shown in Fig. 12 for $\langle v^2 \rangle$ as an example.

These results suggest that neither comparison of the DNS balance errors with the velocity moment values nor with the leading terms in their budgets are capable to detect a loss in the DNS data accuracy observed in the RANS-DNS simulations. Furthermore, such comparisons can be misleading.

When the balance errors are compared to the molecular diffusion terms, the smallest balance terms over a large portion of considered flows, one can observe that the balance errors are extremely large. In Figs. 17a and 17b, such a comparison is shown for $\langle v^2 \rangle$ and $\langle u^2 \rangle$, respectively, in the channel flow⁸. More importantly, the balance errors in such normalization are sensitive to the Reynolds number, increasing with the Reynolds number. This trend is observed for the balance errors in the budgets of all Reynolds stresses, with some dependence on the Reynolds stress at a fixed Reynolds number.

The results shown in Figs. 17a and 17b provide a minimum estimate for the target level of the balance errors when compared with the results of RANS-DNS simulations in Figs. 4-6. That is, the balance errors have to be at least one order of magnitude less than molecular diffusion.

For completeness, the use of turbulent diffusion for the balance error normalization was also examined, and found to be ineffective in accounting for the trends observed in the RANS-DNS simulations. That is, the errors normalized in such a manner are not noticeably affected by variations in the Reynolds number as shown in Figs. 17c and 17d for the $\langle v^2 \rangle$ - and $\langle u^2 \rangle$ - budgets in the channel flow.

In the ZPGBL simulations, the balance error values are two orders of magnitude higher than the molecular diffusion terms (Fig. 18). The variation of Reynolds number is too small in this flow to reveal the dependence of the balance errors on the Reynolds number when normalized by molecular diffusion. Results for the balance errors normalized by the turbulent diffusion are similar to those discussed above for the channel flow and when the errors are normalized by the convective terms. It is worth mentioning that the balance errors in comparison with the turbulent diffusion terms are one order of magnitude higher in a ZPGBL than in the channel flow⁸.

It is of interest to see how the DNS data accuracy changes with increasing the order of velocity moments. The comparison of the balance errors normalized by molecular diffusion from Jeyapaul et al.⁹ (Fig. 19) shows that for all considered moments, the errors are of the same level.

Notice also that normalization by molecular diffusion leads to the same conclusion about the accuracy of different datasets that was previously obtained with normalization by the Reynolds stress values and the leading terms in the Reynolds stress budget. That is, the balance errors from Lee & Moser⁸ are at least one order of magnitude less than those reported in Jeyapaul et al.⁹

Overall, the results presented in Figs. 12-19 demonstrate that the balance errors are not negligible when compared with the other terms in DNS budgets of velocity moments. This explains why physical solutions cannot be obtained from RANS-DNS simulations unless the errors are included in the RANS equations.

The results also lead to the definition of the balance errors small enough, that is, they have to be at least one-two orders of magnitude smaller than the molecular diffusion term in a velocity moment budget. The cost of DNS to obtain such data has yet to be determined. The need for such data is apparent: if one cannot obtain accurate solutions of the RANS equations with DNS data as demonstrated in Figs. 1-9, there are no reliable reference data to validate models for the unknown terms in such equations.

E. Uncertainty quantification metrics

Comparison of the balance terms against molecular diffusion provides a valuable insight into the accuracy of DNS budgets, but in a form of estimates. The stochastic nature of the errors and their dependence on spatial coordinates make it difficult to use them for a quantitative analysis.

Results of RANS-DNS simulations on the other hand are smooth and sensitive to variations in the DNS data inaccuracy. They demonstrate the accuracy of DNS data in an unambiguous manner. Such simulations can be conducted with any reliable solver of the RANS equations in any flow of interest making the procedure easily repeatable and accessible to a broad community.

A difference between the RANS-DNS simulation results and the DNS data for velocity moments is a natural basis for the metrics of uncertainty quantification in the DNS budgets for velocity moments. Multiple uncertainty quantification metrics can be formulated on this basis. One of the simplest possible metrics is based on the L_∞ -norms:

$$\Delta_{\max} = \frac{|g(y) - f(y)|_{\infty}}{|g(y)|_{\infty}}, \quad (9)$$

where $g(y)$ represents DNS data for a velocity moment, and $f(y)$ is the solution obtained from RANS-DNS simulations for this moment.

Table 3. Values of Δ_{\max} describing the accuracy of DNS budgets from Lee & Moser⁸ (in %).

Δ_{\max}	$\langle u^2 \rangle$	$\langle v^2 \rangle$	$\langle uv \rangle$	$\langle w^2 \rangle$
$Re_{\tau} = 180$	6	5	5	13
$Re_{\tau} = 550$	10	17	21	20
$Re_{\tau} = 5200$	287	548	173	308

Table 4. Values of Δ_{\max} describing the accuracy of DNS budgets from Jeyapaul⁹ et al. (in %).

	$\langle u^2 \rangle$	$\langle v^2 \rangle$	$\langle uv \rangle$	$\langle w^2 \rangle$
Δ_{\max}	164	663	629	507
	$\langle u^3 \rangle$	$\langle v^3 \rangle$	$\langle uv^2 \rangle$	$\langle u^2v \rangle$
Δ_{\max}	625	1290	1170	243
	$\langle u^4 \rangle$	$\langle v^4 \rangle$	$\langle uv^3 \rangle$	$\langle u^3v \rangle$
Δ_{\max}	125	1970	474	354

Table 5. Values of Δ_{\max} describing the accuracy of DNS budgets from Sillero et al.¹⁰ (in %).

Δ_{\max}	$\langle u^2 \rangle$	$\langle v^2 \rangle$	$\langle uv \rangle$	$\langle w^2 \rangle$
$Re_{\theta} = 4500$	2793	3635	2177	1998
$Re_{\theta} = 6000$	4464	4532	2723	3793

Tables 3-5 show the values of Δ_{\max} corresponding to the results discussed previously. These results confirm the general observations made from the analysis of the balance errors. That is, all

results from RANS-DNS simulations, which were received without taking into account the balance errors, are unphysical with the exception of those in the channel flow at $Re_\tau = 180$ and 550 obtained with the DNS data from Lee & Moser⁸. In these two flows, $\Delta_{\max} < 100\%$. The errors grow with the Reynolds number in the channel flow⁸ and in a ZPGBL¹⁰. The errors in the DNS budgets from Lee & Moser⁸ are the smallest from the three considered datasets. At the closest Reynolds numbers in the channel flow, the errors from Lee & Moser⁸ are at least one order of magnitude smaller than those from Jeyapaul et al.⁹. No particular growth in the errors is observed with increasing the order of velocity moments. Exceptions are the moments with the increasing power of the velocity fluctuation v in the direction normal to the wall (Table 5) such as, for example, $\langle v^2 \rangle$, $\langle v^3 \rangle$, and $\langle v^4 \rangle$.

The later observation was not apparent from the analysis of balance errors presented above. Also, the analysis of balance errors did not reveal that the errors in the DNS budgets of $\langle v^2 \rangle$ tend to be much higher than the errors in the budgets of other Reynolds stresses at higher Reynolds numbers (Tables 3 and 5). The recommended threshold for Δ_{\max} when collected statistics from DNS is 5%. Overall, the proposed metric is a simple, accurate, and reliable criterion to be used for evaluating the accuracy of DNS budgets.

Other metrics integrated over y can also be used, but whether they will be a better fit for the task is a subject for future studies as additional DNS data are required for a conclusive analysis.

V. CONCLUSIONS

The results of RANS-DNS simulations presented in the paper demonstrate that inaccuracies in the DNS budgets used in the simulations are the dominant source of uncertainty in the simulation results, whereas uncertainties introduced by a numerical procedure employed for simulations have

no recognizable effect. This makes the RANS-DNS simulations a plausible framework for quantifying the total uncertainty in statistical data collected from DNS.

The RANS-DNS simulations conducted with the data from three DNS datasets⁸⁻¹⁰ in the channel flow and in a ZPGBL revealed that with the exception of data⁸ at the lowest Reynolds number in the channel flow, $Re_\tau = 180$, the balance errors in the DNS budgets are too high, leading to unphysical simulation results. This is in spite of the use of standard and advanced uncertainty quantification procedures^{3,5,6} when collecting the data.

The conducted analysis of the balance errors in DNS budgets revealed that for the balance errors to be small enough, they have to be at least the order of magnitude smaller than the molecular diffusion terms. The analysis also demonstrated that comparison with the leading terms in DNS budgets as well as directly with the velocity moments may be misleading in evaluation of the data accuracy.

The analysis of the balance errors although informative, gives only qualitative estimates. A metric based on comparison of the results of RANS-DNS simulations with the DNS data for the corresponding velocity moments is proposed for a quantitative analysis of the DNS budget accuracy. Rigor of the proposed uncertainty quantification procedure, availability of reliable RANS solvers, and low computational cost of such simulations makes the proposed approach for evaluating the DNS data accuracy accessible and attractive to a broad community.

ACKNOWLEDGMENTS

A part of the presented material is based upon work supported by National Aeronautics and Space Administration under award NNX12AJ61A. High-performance computing facilities of the

Center for Advance Research Computing at the University of New Mexico were also used in the study.

REFERENCES

- ¹T. J. Barth, “An Overview of Combined Uncertainty and A Posteriori Error Bound Estimates for CFD Calculations,” AIAA2016-1062, Proc. AIAA SciTech, San Diego, CA, January 4-8 (2016).
- ²S. A. Orszag, “Numerical Simulation of Incompressible Flows Within Simple Boundaries: Accuracy,” J. Fluids Mech., **49** (1), 75-112 (1971).
- ³N. N. Mansour, J. Kim, and P. Moin, “Reynolds-stress and dissipation-rate budgets in a turbulent channel flow,” J. Fluid Mech., **194**, 15-44 (1988).
- ⁴R. S. Rogallo, “Numerical Experiments in Homogeneous Turbulence,” NASA TM-81315 (1981).
- ⁵S. Hoyas and J. Jiménez, “Reynolds Number Effects on the Reynolds-stress Budgets in Turbulent Channels,” Phys. Fluids, **20**, 100511 (2008).
- ⁶T. A. Oliver, N. Malaya, R. Ulerich, and R. D. Moser, “Estimating uncertainties in statistics computed from direct numerical simulation,” Phys. Fluids, **26** (3), 035101 (2014).
- ⁷P. J. Roache, *Verification and Validation in Computational Sciences and Engineering* (Hermosa Publishers, 1998).
- ⁸M. Lee, R. D. Moser, "Direct numerical simulation of turbulent channel flow up to $Re_{\tau} = 5200$ ", J. Fluid Mech., **774**, 395-415, <http://turbulence.ices.utexas.edu/> (2015).
- ⁹E. Jeyapaul, G. N. Coleman, C. L. Rumsey, “Higher-order and length-scale statistics from DNS of a decelerated planar wall-bounded turbulent flow,” Int. J. Heat and Fluid Flow, **54**, 14-27 (2015).
- ¹⁰J. A. Sillero, J. Jiménez, and R. D. Moser, “One-Point Statistics for Turbulent Wall-Bounded Flows at Reynolds Numbers up to $\delta^+ = 2000$,” Phys. Fluids, **25**(10), 1-15 (2013).
- ¹¹OpenFOAM, Open-source Field Operation & Manipulation, Software Pack., Ver. 2.3.0 URL: <http://www.openfoam.com/> (2014)
- ¹²D. B., Spalding, *GENMIX: A General Computer Program for Two-Dimensional Parabolic Phenomena* (Pergamon, N, 1977).
- ¹³M. D. Buhmann, *Radial Basis Functions: Theory and Implementations* (Cambridge University Press, 2003).

¹⁴S. V. Poroseva, J. D. Colmenares F., S. M. Murman, "RANS Simulations of a Channel Flow with a New Velocity/Pressure-Gradient Model," AIAA2015-3067, Proc. AIAA Aviation 2015, Dallas, TX, June 22-25 (2015).

APPENDIX

Here, the exact RANS equations in planar incompressible turbulent flows are provided. The equations for the mean flow velocity components are:

$$\begin{aligned} \frac{\partial U}{\partial t} + U \frac{\partial U}{\partial x} + V \frac{\partial U}{\partial y} &= -\frac{1}{\rho} \frac{\partial \bar{P}}{\partial x} - \frac{\partial \langle u^2 \rangle}{\partial x} - \frac{\partial \langle uv \rangle}{\partial y} + \nu \frac{\partial^2 U}{\partial x^2} + \nu \frac{\partial^2 U}{\partial y^2}, \\ \frac{\partial V}{\partial t} + U \frac{\partial V}{\partial x} + V \frac{\partial V}{\partial y} &= -\frac{1}{\rho} \frac{\partial \bar{P}}{\partial y} - \frac{\partial \langle uv \rangle}{\partial x} - \frac{\partial \langle v^2 \rangle}{\partial y} + \nu \frac{\partial^2 V}{\partial x^2} + \nu \frac{\partial^2 V}{\partial y^2}, \end{aligned} \quad (\text{A1})$$

$$\frac{\partial U}{\partial x} + \frac{\partial V}{\partial y} = 0,$$

where x and y are coordinates in the streamwise and normal-to-the-wall directions, respectively; U and V are the mean velocity components in the x and y -directions; u and v are the turbulent velocity fluctuations in the same directions; \bar{P} is the mean pressure; ρ is the density, and ν is the kinematic viscosity.

The transport equation for velocity moment $\langle u^n v^m w^k \rangle$ of an arbitrary order is the following:

$$\begin{aligned}
& \frac{\partial \langle u^n v^m w^k \rangle}{\partial t} + U \frac{\partial \langle u^n v^m w^k \rangle}{\partial x} + V \frac{\partial \langle u^n v^m w^k \rangle}{\partial y} = \nu \left[\frac{\partial^2 \langle u^n v^m w^k \rangle}{\partial x^2} + \frac{\partial^2 \langle u^n v^m w^k \rangle}{\partial y^2} \right] + \\
& + (m-n) \langle u^n v^m w^k \rangle \frac{\partial U}{\partial x} - n \langle u^{n-1} v^{m+1} w^k \rangle \frac{\partial U}{\partial y} - m \langle u^{n+1} v^{m-1} w^k \rangle \frac{\partial V}{\partial x} + \\
& + n \langle u^{n-1} v^m w^k \rangle \left[\frac{\partial \langle u^2 \rangle}{\partial x} + \frac{\partial \langle uv \rangle}{\partial y} \right] + m \langle u^n v^{m-1} w^k \rangle \left[\frac{\partial \langle v^2 \rangle}{\partial y} + \frac{\partial \langle uv \rangle}{\partial x} \right] - \\
& - \frac{\partial \langle u^{n+1} v^m w^k \rangle}{\partial x} - \frac{\partial \langle u^n v^{m+1} w^k \rangle}{\partial y} - \frac{1}{\rho} \left[n \langle u^{n-1} v^m w^k \frac{\partial p}{\partial x} \rangle + m \langle u^n v^{m-1} w^k \frac{\partial p}{\partial y} \rangle + k \langle u^n v^{m-1} w^{k-1} \frac{\partial p}{\partial z} \rangle \right] + \\
& - 2\nu m k \langle u^n v^{m-1} w^{k-1} \left[\frac{\partial v}{\partial x} \frac{\partial w}{\partial x} + \frac{\partial v}{\partial y} \frac{\partial w}{\partial y} + \frac{\partial v}{\partial z} \frac{\partial w}{\partial z} \right] \rangle - 2\nu n k \langle u^{n-1} v^m w^{k-1} \left[\frac{\partial u}{\partial x} \frac{\partial w}{\partial x} + \frac{\partial u}{\partial y} \frac{\partial w}{\partial y} + \frac{\partial u}{\partial z} \frac{\partial w}{\partial z} \right] \rangle - \\
& - 2\nu n m \langle u^{n-1} v^{m-1} w^k \left[\frac{\partial u}{\partial x} \frac{\partial v}{\partial x} + \frac{\partial u}{\partial y} \frac{\partial v}{\partial y} + \frac{\partial u}{\partial z} \frac{\partial v}{\partial z} \right] \rangle - \nu n(n-1) \langle u^{n-2} v^m w^k \left[\left(\frac{\partial u}{\partial x} \right)^2 + \left(\frac{\partial u}{\partial y} \right)^2 + \left(\frac{\partial u}{\partial z} \right)^2 \right] \rangle - \\
& - \nu m(m-1) \langle u^n v^{m-2} w^k \left[\left(\frac{\partial v}{\partial x} \right)^2 + \left(\frac{\partial v}{\partial y} \right)^2 + \left(\frac{\partial v}{\partial z} \right)^2 \right] \rangle - \nu k(k-1) \langle u^n v^m w^{k-2} \left[\left(\frac{\partial w}{\partial x} \right)^2 + \left(\frac{\partial w}{\partial y} \right)^2 + \left(\frac{\partial w}{\partial z} \right)^2 \right] \rangle.
\end{aligned} \tag{A2}$$

Additional notations are: w is the turbulent velocity fluctuation in the spanwise direction, z , and p is the pressure fluctuation; integers n , m , and k run from 0 to infinity, with $n + m + k \geq 2$. Terms like $\langle \dots u_i^{s-t} \dots \rangle$ do not contribute in the transport equations for velocity moments with $s < t$.

In (A2), terms representing the viscous diffusion and the turbulent diffusion are

$$\mathbf{D}^M = \nu \left[\frac{\partial^2 \langle u^n v^m w^k \rangle}{\partial x^2} + \frac{\partial^2 \langle u^n v^m w^k \rangle}{\partial y^2} \right],$$

$$\mathbf{D}^T = -\frac{\partial \langle u^{n+1} v^m w^k \rangle}{\partial x} - \frac{\partial \langle u^n v^{m+1} w^k \rangle}{\partial y},$$

respectively. Other terms are the viscous dissipation $\boldsymbol{\varepsilon}$ (viscous terms not relevant to the viscous diffusion), production-by-strain, \mathbf{P} , with the mean velocity gradients and the production-by-turbulence, \mathbf{P}^T , with the Reynolds stress gradients. The production-by-turbulence terms appear in the transport equations for velocity moments of the third and higher orders. Terms with the pressure fluctuation gradients are the velocity/pressure-gradient correlations, $\boldsymbol{\Pi}$, representing the interaction of turbulent velocity and pressure fluctuation fields.

FIGURES

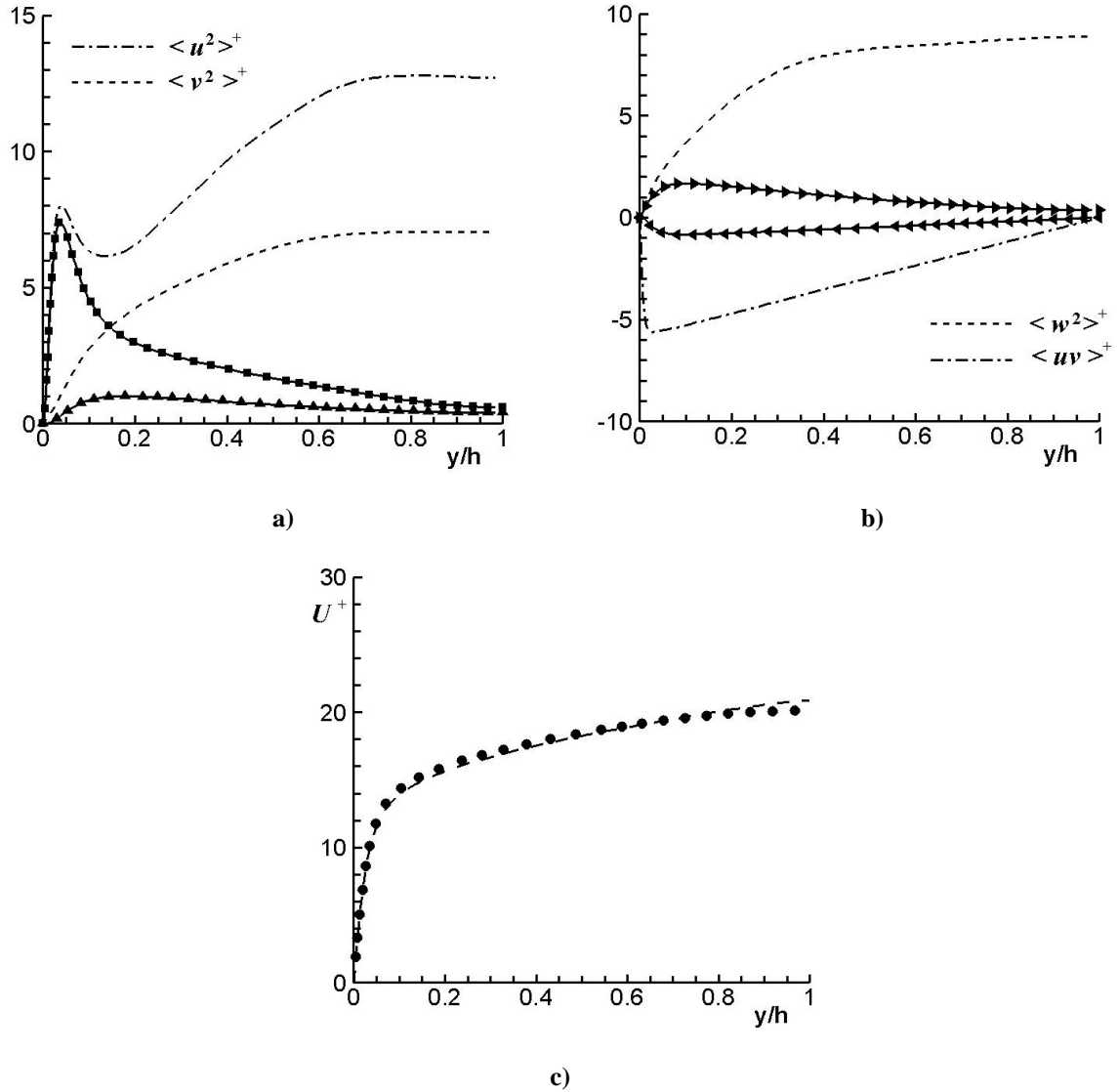


FIG. 1. The Reynolds stresses and the mean flow velocity in a fully-developed turbulent channel flow at $Re_\tau = 392$: $\blacksquare \langle u^2 \rangle^+$, $\blacktriangle \langle v^2 \rangle^+$, $\blacktriangleright \langle w^2 \rangle^+$, $\blacktriangleleft \langle uv \rangle^+$, $\bullet U$ DNS⁹; ---, - . - RANS-DNS simulations with equation (1) and the transport equation for the mean flow velocity; — RANS-DNS simulations with equation (5).

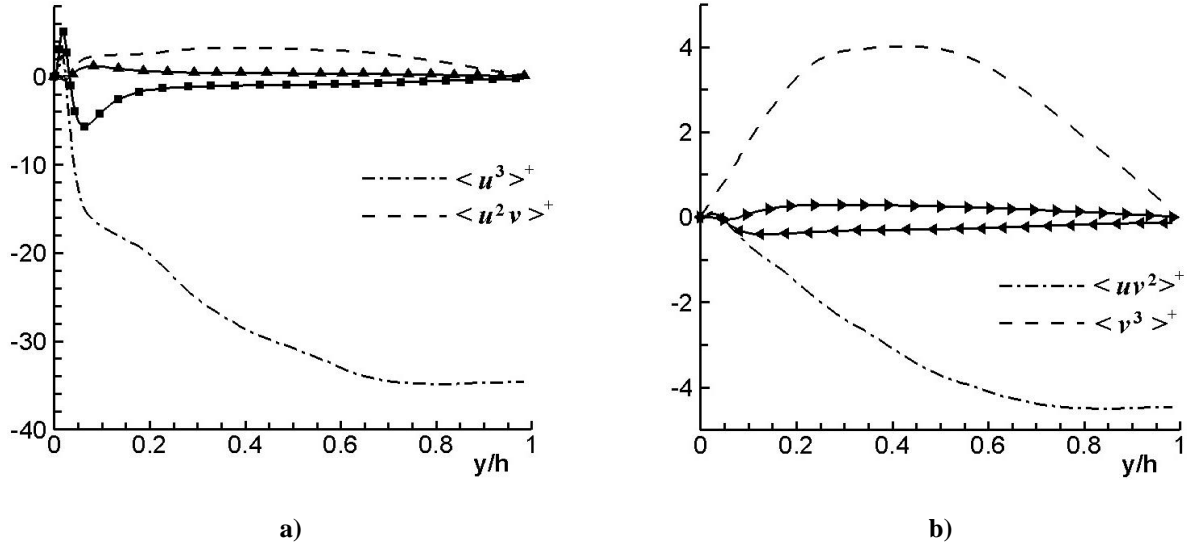


FIG. 2. The third-order velocity moments in a fully-developed turbulent channel flow at $Re_\tau = 392$: \blacksquare $\langle u^3 \rangle^+$, \blacktriangle $\langle u^2 v \rangle^+$, \blacktriangleright $\langle v^3 \rangle^+$, \blacktriangleleft $\langle uv^2 \rangle^+$ DNS; ---, - . - RANS-DNS simulations with equation (2); — RANS-DNS simulations with equation (6).

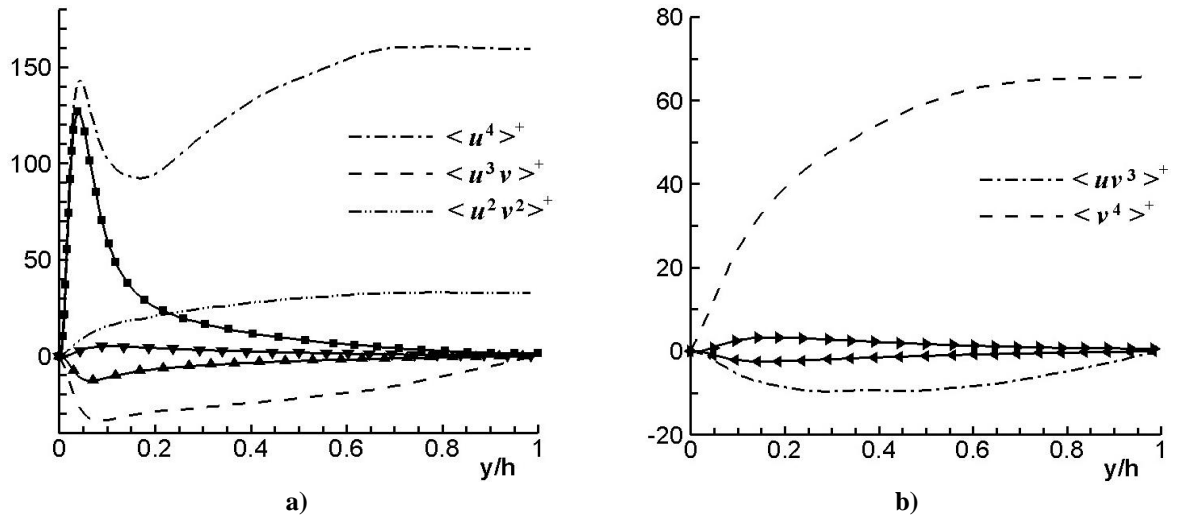


FIG. 3. The fourth-order velocity moments in a fully-developed turbulent channel flow at $Re_\tau = 392$: \blacksquare $\langle u^4 \rangle^+$, \blacktriangle $\langle u^3 v \rangle^+$, \blacktriangledown $\langle u^2 v^2 \rangle^+$, \blacktriangleright $\langle v^4 \rangle^+$, \blacktriangleleft $\langle uv^3 \rangle^+$ DNS; ---, - · -, and - · · - RANS-DNS simulations with equation (3); — RANS-DNS simulations with equation (7).

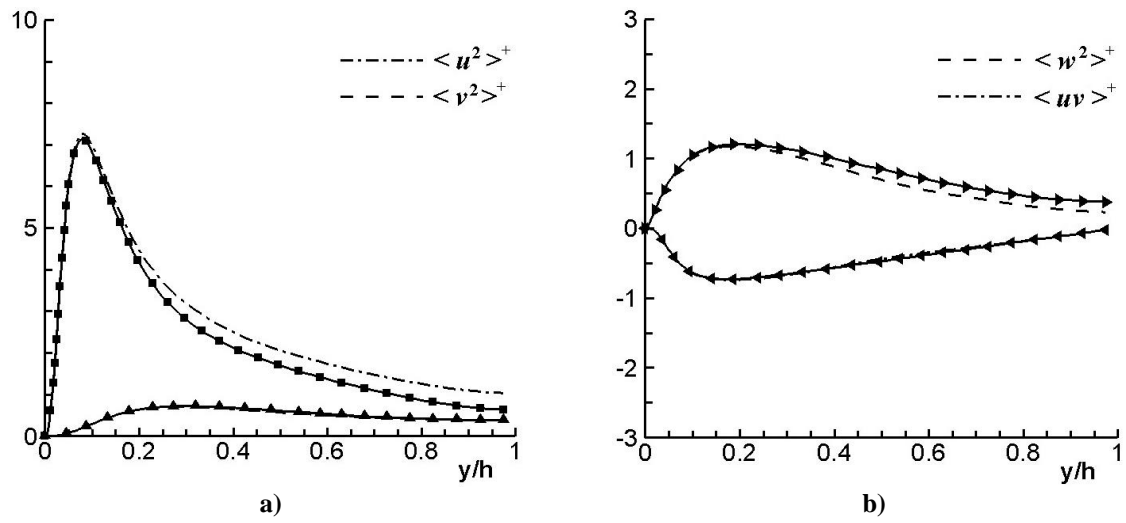


FIG. 4. The Reynolds stresses in a fully-developed turbulent channel flow at $Re_\tau = 180$: \blacksquare $\langle u^2 \rangle^+$, \blacktriangle $\langle v^2 \rangle^+$, \blacktriangleright $\langle w^2 \rangle^+$, \blacktriangleleft $\langle uv \rangle^+$ DNS⁸; ---, - · - RANS-DNS simulations with equation (1); — RANS-DNS simulations with equation (5).

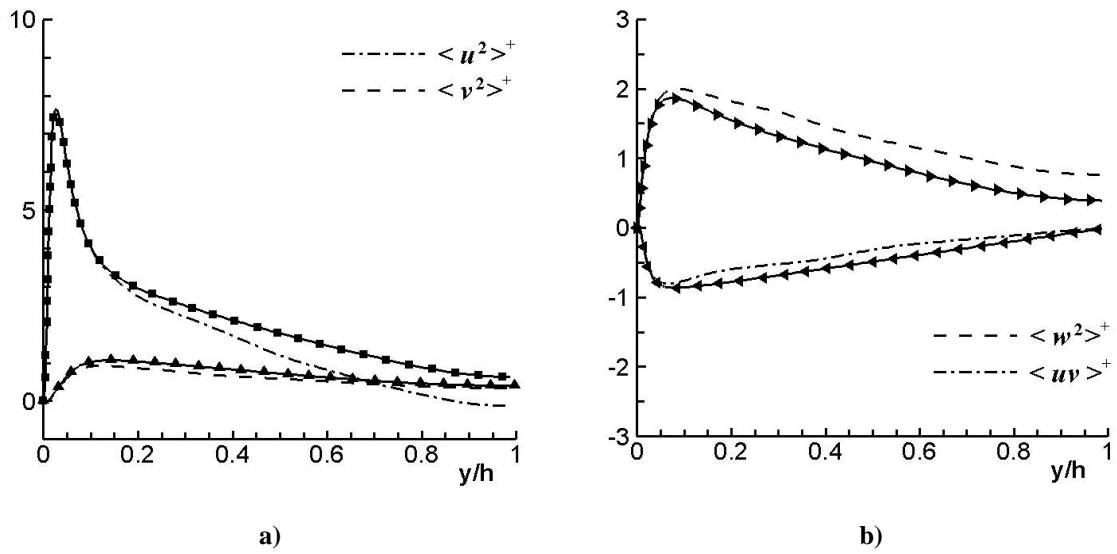


FIG. 5. The Reynolds stresses in a fully-developed turbulent channel flow at $Re_\tau = 550$: \blacksquare $\langle u^2 \rangle$, \blacktriangle $\langle v^2 \rangle$, \blacktriangleright $\langle w^2 \rangle$, \blacktriangleleft $\langle uv \rangle$ DNS⁸; ---, - - - RANS-DNS simulations with equation (1); — RANS-DNS simulations with equation (5).

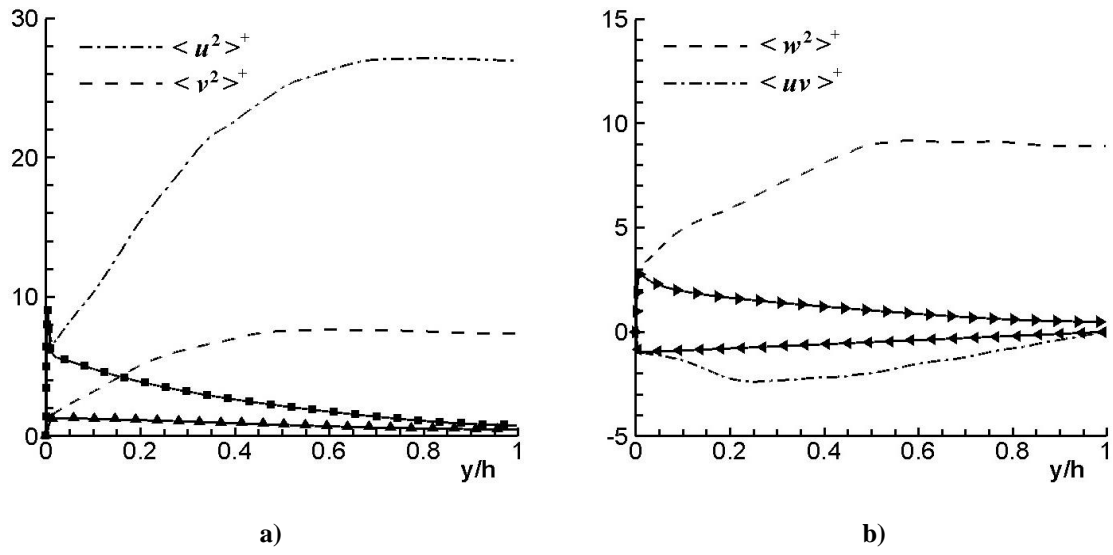


FIG. 6. The Reynolds stresses in a fully-developed turbulent channel flow at $Re_\tau = 5200$: ■ $\langle u^2 \rangle^+$, ▲ $\langle v^2 \rangle^+$, ► $\langle w^2 \rangle^+$, ◄ $\langle uv \rangle^+$ DNS⁸; ---, - · - RANS-DNS simulations with equation (1); — RANS-DNS simulations with equation (5).

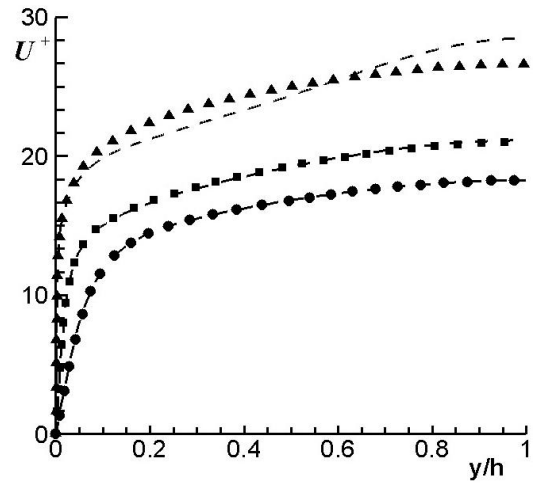


FIG. 7. The mean flow velocity in a fully-developed turbulent channel flow: --- RANS-DNS simulations; ● $Re_{\tau} = 180$, ■ $Re_{\tau} = 550$, ▲ $Re_{\tau} = 5200$ DNS⁸.

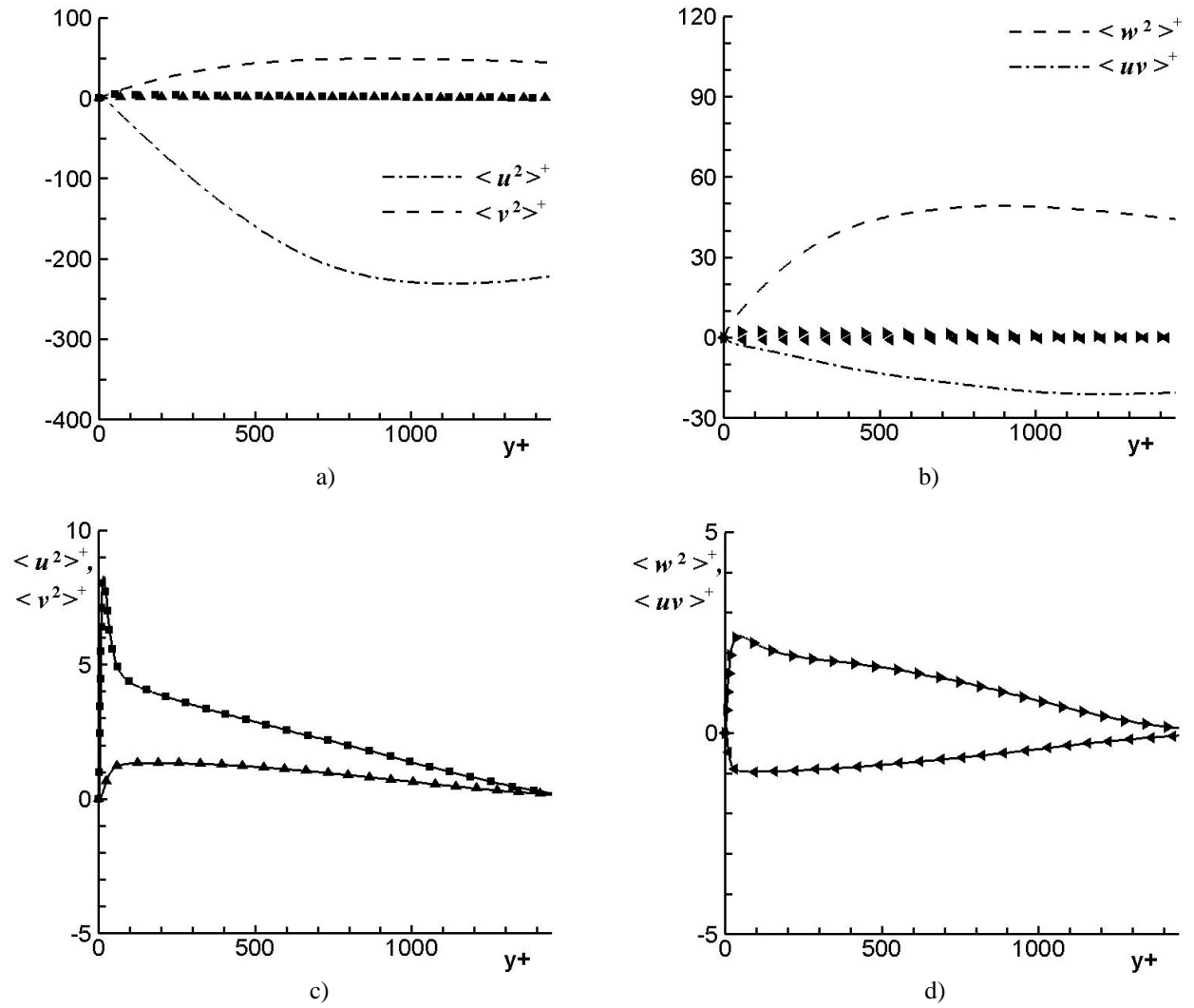


FIG. 8. The Reynolds stresses in a ZPGBL at $Re_\theta = 4500$: ■ $\langle u^2 \rangle^+$, ▲ $\langle v^2 \rangle^+$; ► $\langle w^2 \rangle^+$, ◄ $\langle uv \rangle^+$ DNS¹⁰; - - -, - - - RANS-DNS simulations with equation (4); — RANS-DNS simulations with equation (8).

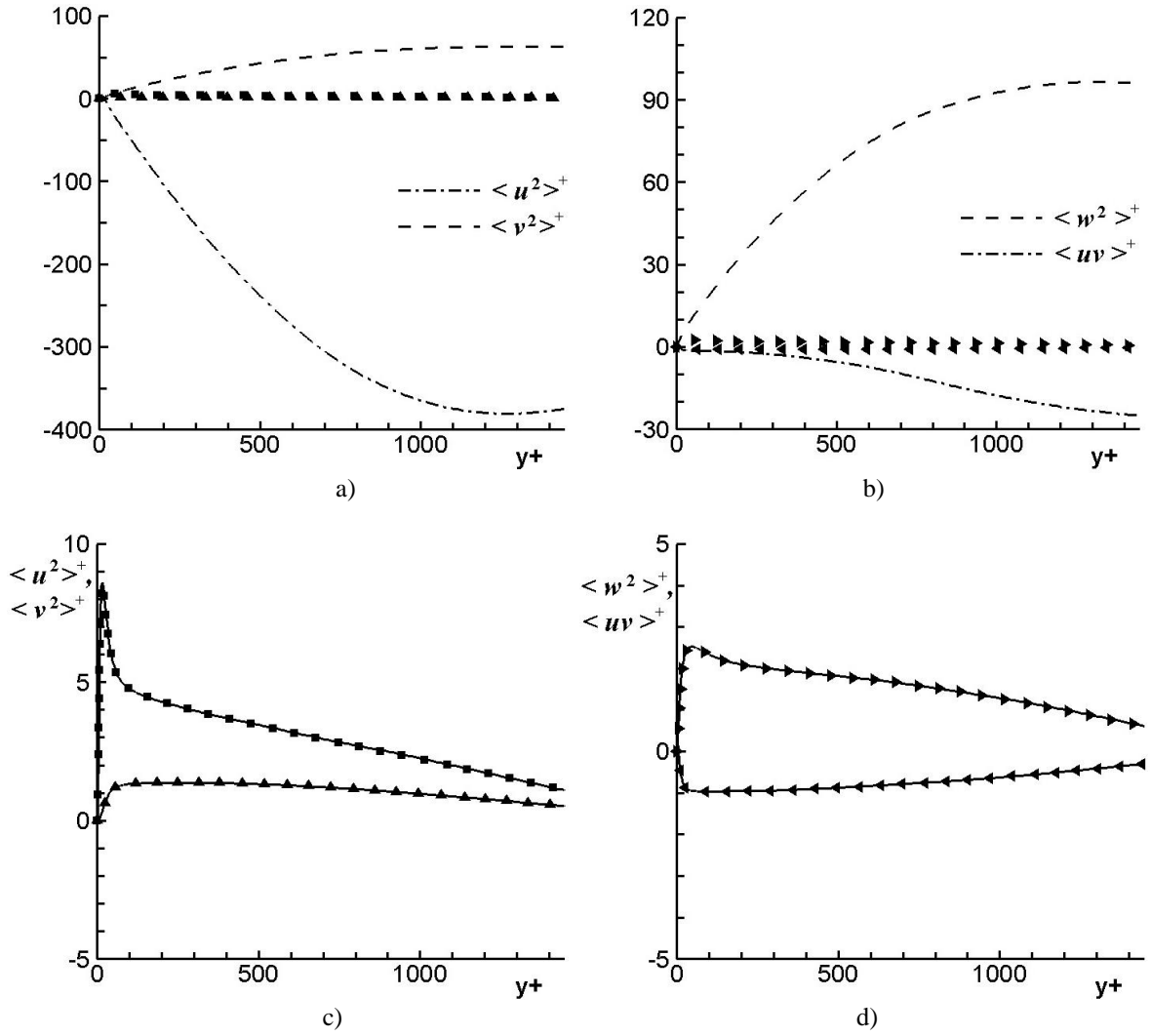


FIG. 9. The Reynolds stresses in a ZPGBL at $Re_\theta = 6000$: ■ $\langle u^2 \rangle^+$, ▲ $\langle v^2 \rangle^+$, ► $\langle w^2 \rangle^+$, ◄ $\langle uv \rangle^+$ DNS¹⁰; ---, - · - RANS-DNS simulations with equation (4); — RANS-DNS simulations with equation (8).

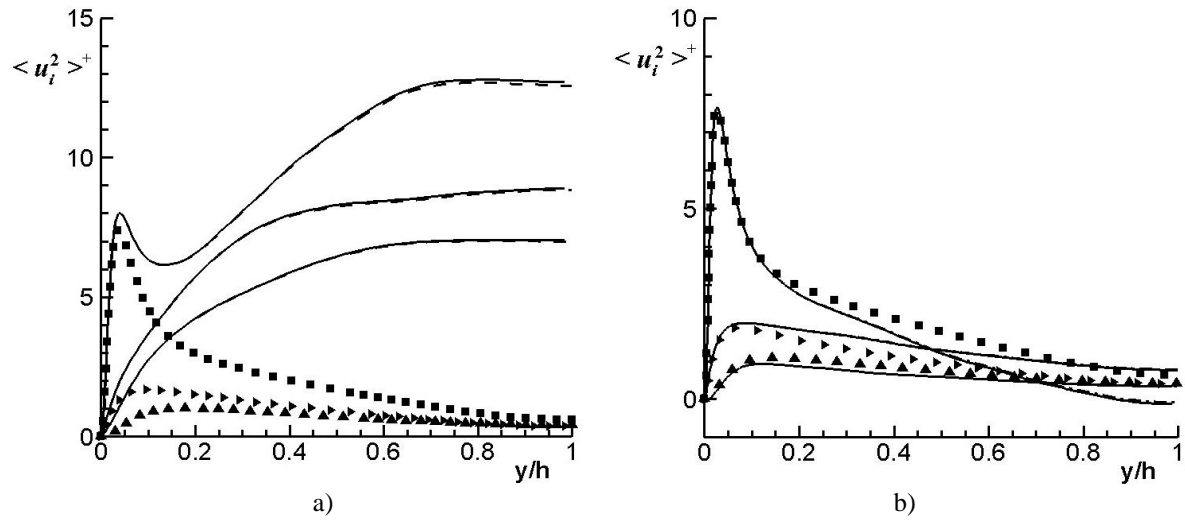


FIG. 10. The Reynolds stresses in a fully-developed turbulent channel flow obtained from RANS-DNS simulations using a) different solvers, b) different interpolation schemes. Notations: a) $\blacksquare \langle u^2 \rangle$, $\blacktriangle \langle v^2 \rangle$, $\blacktriangleright \langle w^2 \rangle$ DNS⁹; --- the in-house code; — OpenFOAM; b) $\blacksquare \langle u^2 \rangle$, $\blacktriangle \langle v^2 \rangle$, $\blacktriangleright \langle w^2 \rangle$ DNS⁸ at $Re_\tau = 550$, — cubic splines, --- quadratic splines, - · - radial basis functions.

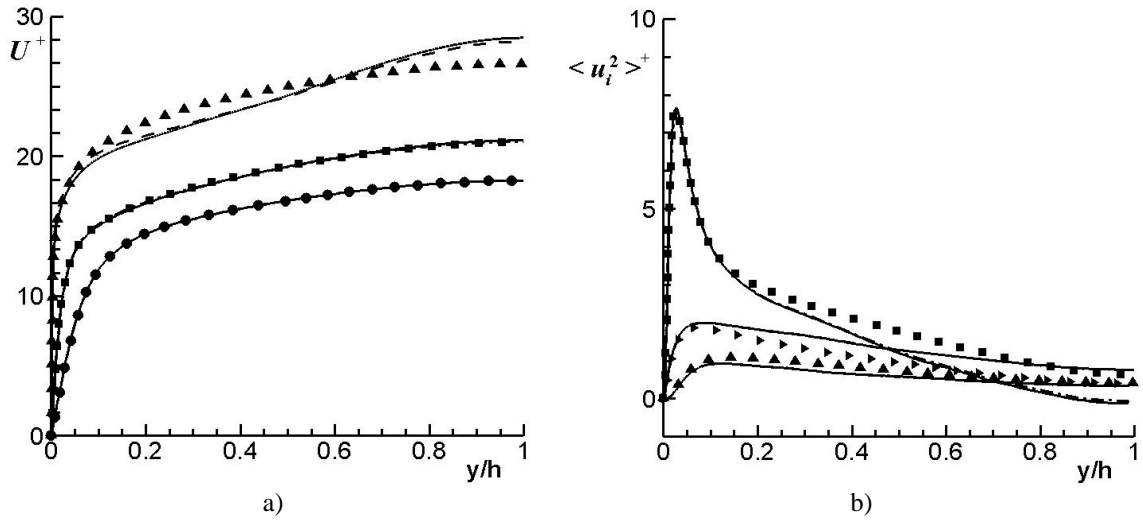


FIG. 11. The grid resolution effect in RANS-DNS simulations in a fully-developed turbulent channel flow with DNS data⁸: a) mean flow velocities at three Reynolds numbers, b) Reynolds stresses. DNS profiles: a) ● $Re_\tau = 180$, ■ $Re_\tau = 550$, ▲ $Re_\tau = 5200$; b) ■ $\langle u^2 \rangle^+$, ▲ $\langle v^2 \rangle^+$, ● $\langle w^2 \rangle^+$ at $Re_\tau = 550$. RANS-DNS simulations: — native grids from DNS⁸ (Table 2): $N_y = 191$ ($Re_\tau = 180$), $N_y = 383$ ($Re_\tau = 550$), and $N_y = 1535$ ($Re_\tau = 5200$); --- grid from DNS⁹: $N_y = 193$ (for all Re_τ); - · - grid with $N_y = 97$ ($Re_\tau = 550$).

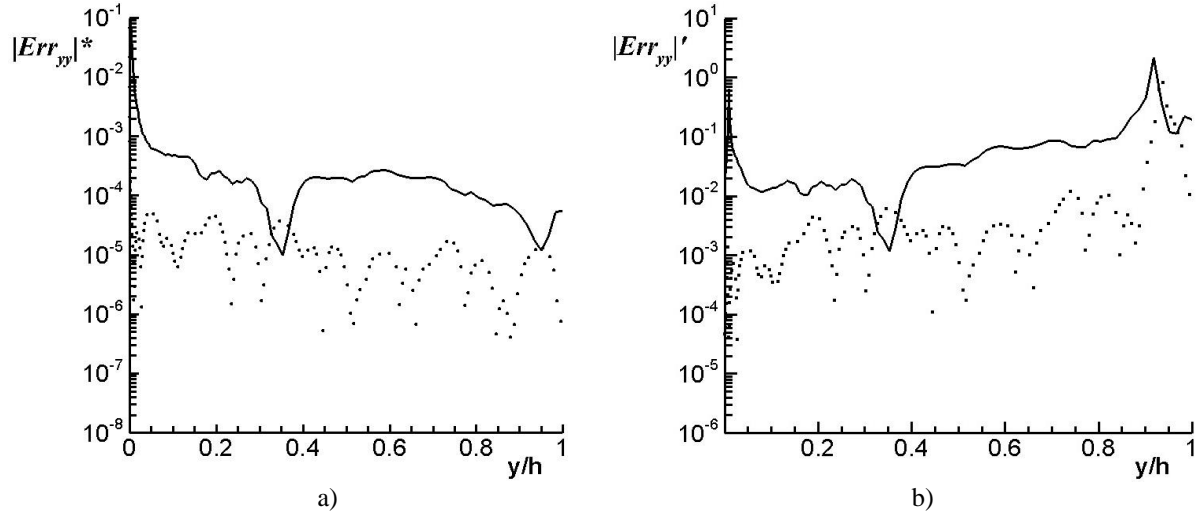


FIG. 12. Normalized absolute values of the DNS balance errors for $\langle v^2 \rangle$ in the channel flow: a) $|Err_{yy}|^* = |Err_{yy}| / \langle v^2 \rangle$, b) $|Err_{yy}|' = |Err_{yy}| / \Pi_{yy}$. Notations: — Jeyapaul et al.⁹ ($Re_\tau = 392$), ••• Lee & Moser⁸ ($Re_\tau = 550$).

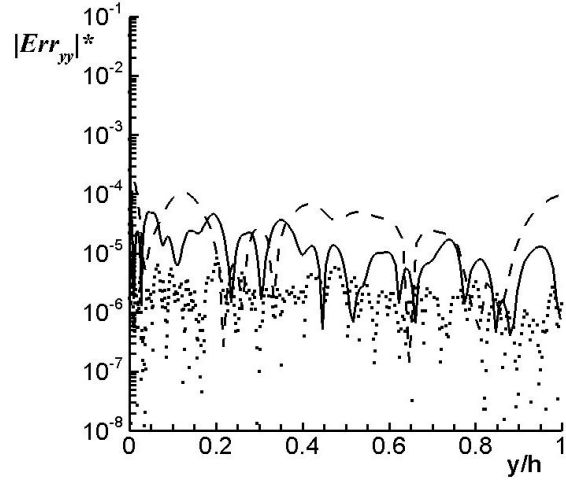


FIG. 13. Normalized absolute values of the DNS⁸ balance errors $|Err_{yy}|^* = |Err_{yy}| / \langle v^2 \rangle$ in the channel flow. Notations: --- $Re_\tau = 180$, — $Re_\tau = 550$, ··· $Re_\tau = 5200$.

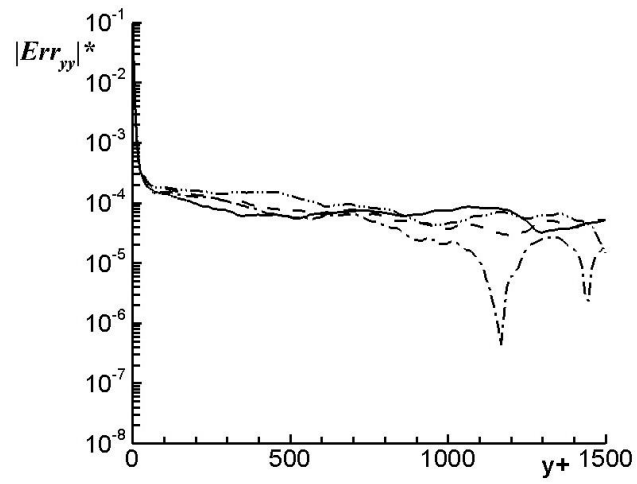


Fig. 14. Normalized absolute values of the DNS¹⁰ balance errors $|Err_{yy}|^* = |Err_{yy}| / \langle v^2 \rangle$ in a ZPGBL. Notations: $- \cdot -$ $Re_\theta = 4500$, $- - -$ $Re_\theta = 5000$, $- \cdot - \cdot -$ $Re_\theta = 5500$, $—$ $Re_\theta = 6000$.

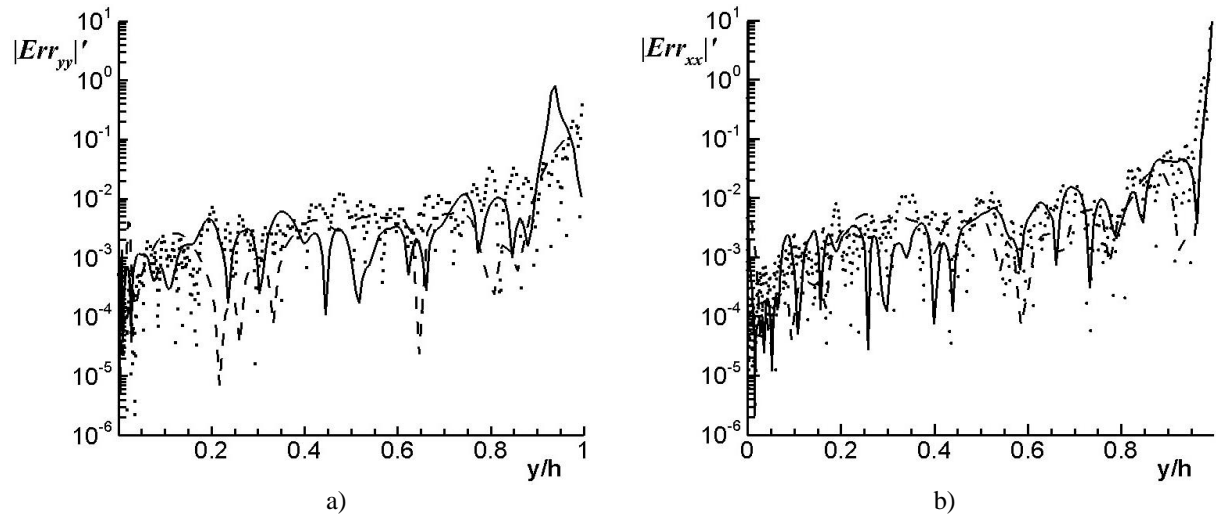


FIG. 15. Ratio of the balance errors to the leading terms, $|Err_{\alpha\alpha}'|$, in the DNS⁸ budgets of the Reynolds stresses in the channel flow: a) $|Err_{yy}'| = |Err_{yy}/\Pi_{yy}|$, b) $|Err_{xx}'| = |Err_{xx}/P_{xx}|$. Notations: - - - $Re_{\tau} = 180$, — $Re_{\tau} = 550$, ••• $Re_{\tau} = 5200$.

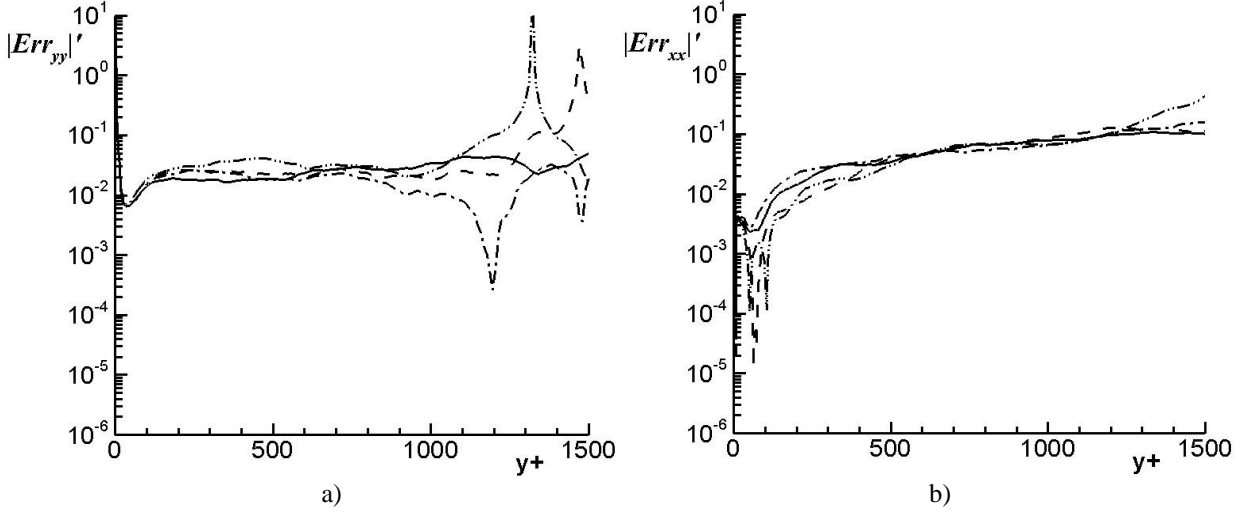


FIG. 16. Ratio of the balance errors to the leading terms, $|Err_{\alpha\alpha}|'$, in the DNS¹⁰ budgets of the Reynolds stresses in a ZPGBL: a) $|Err_{yy}|' = |Err_{yy}/\Pi_{yy}|$, b) $|Err_{xx}|' = |Err_{xx}/P_{xx}|$. Notations: $-\cdot-\cdot-$ $Re_{\theta} = 4500$, $----$ $Re_{\theta} = 5000$, $-\cdot-\cdot-$ $Re_{\theta} = 5500$, $—$ $Re_{\theta} = 6000$.

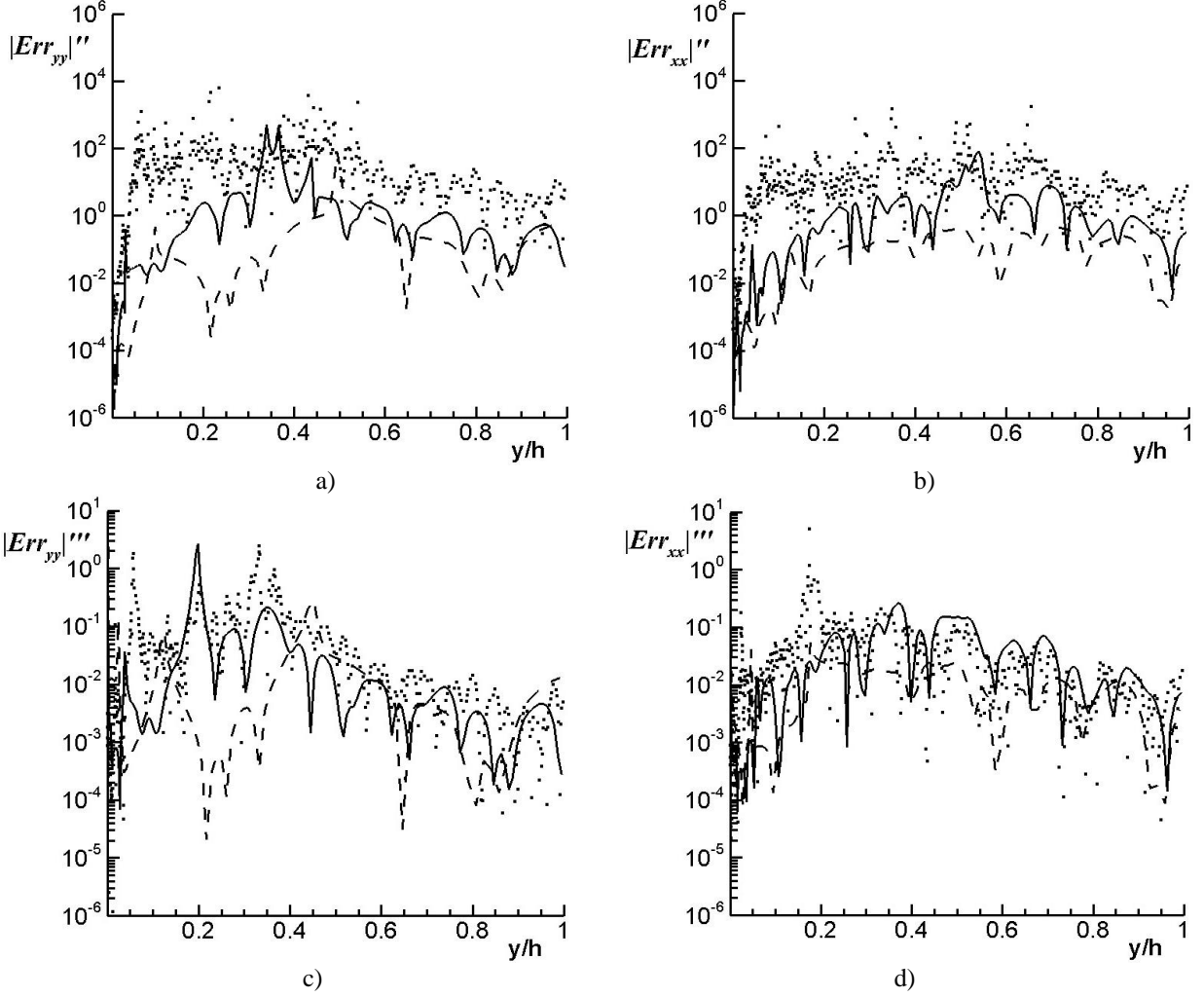


FIG. 17. Ratios of the balance errors to molecular and turbulent diffusion terms, $|Err_{\alpha\alpha}|'' = |Err_{\alpha\alpha}/D_{\alpha\alpha}^M|$ and $|Err_{\alpha\alpha}|''' = |Err_{\alpha\alpha}/D_{\alpha\alpha}^T|$, in the DNS⁸ budgets of the Reynolds stresses in the channel flow: a) $|Err_{yy}|''$, b) $|Err_{xx}|''$, c) $|Err_{yy}|'''$, d) $|Err_{xx}|'''$. Notations: --- $Re_\tau = 180$, — $Re_\tau = 550$, ··· $Re_\tau = 5200$.

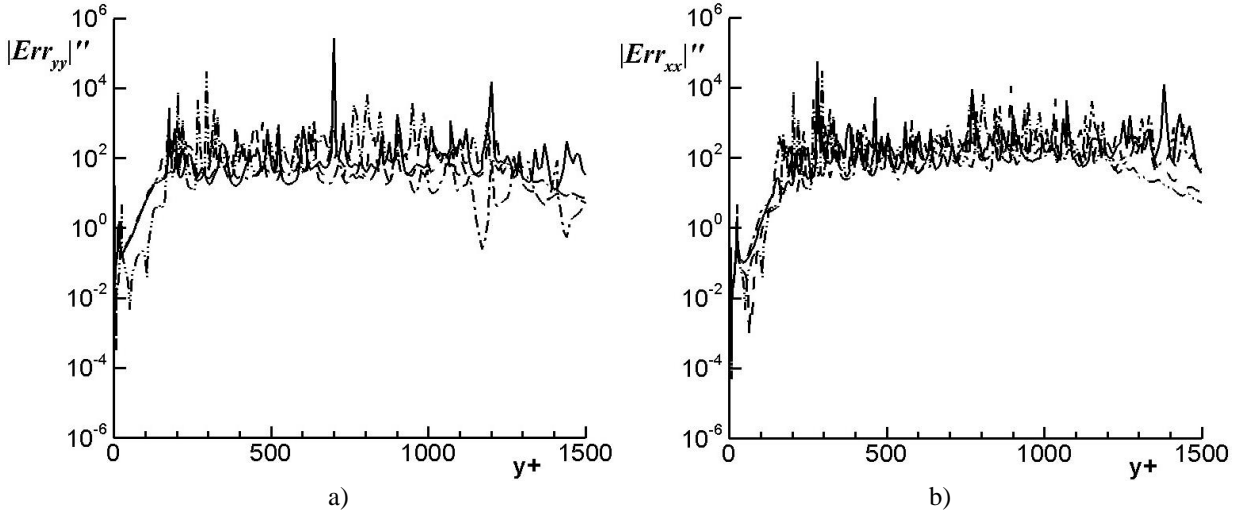


FIG. 18. Ratio of the balance errors to the molecular diffusion terms, $|Err_{\alpha\alpha}|'' = |Err_{\alpha\alpha} / D_{\alpha\alpha}^M|$, in the DNS¹⁰ budgets of the Reynolds stresses in a ZPGBL: a) $|Err_{yy}|''$, b) $|Err_{xx}|''$. Notations: - · · - $Re_\theta = 4500$, - - - $Re_\theta = 5000$, - · · - $Re_\theta = 5500$, — $Re_\theta = 6000$.

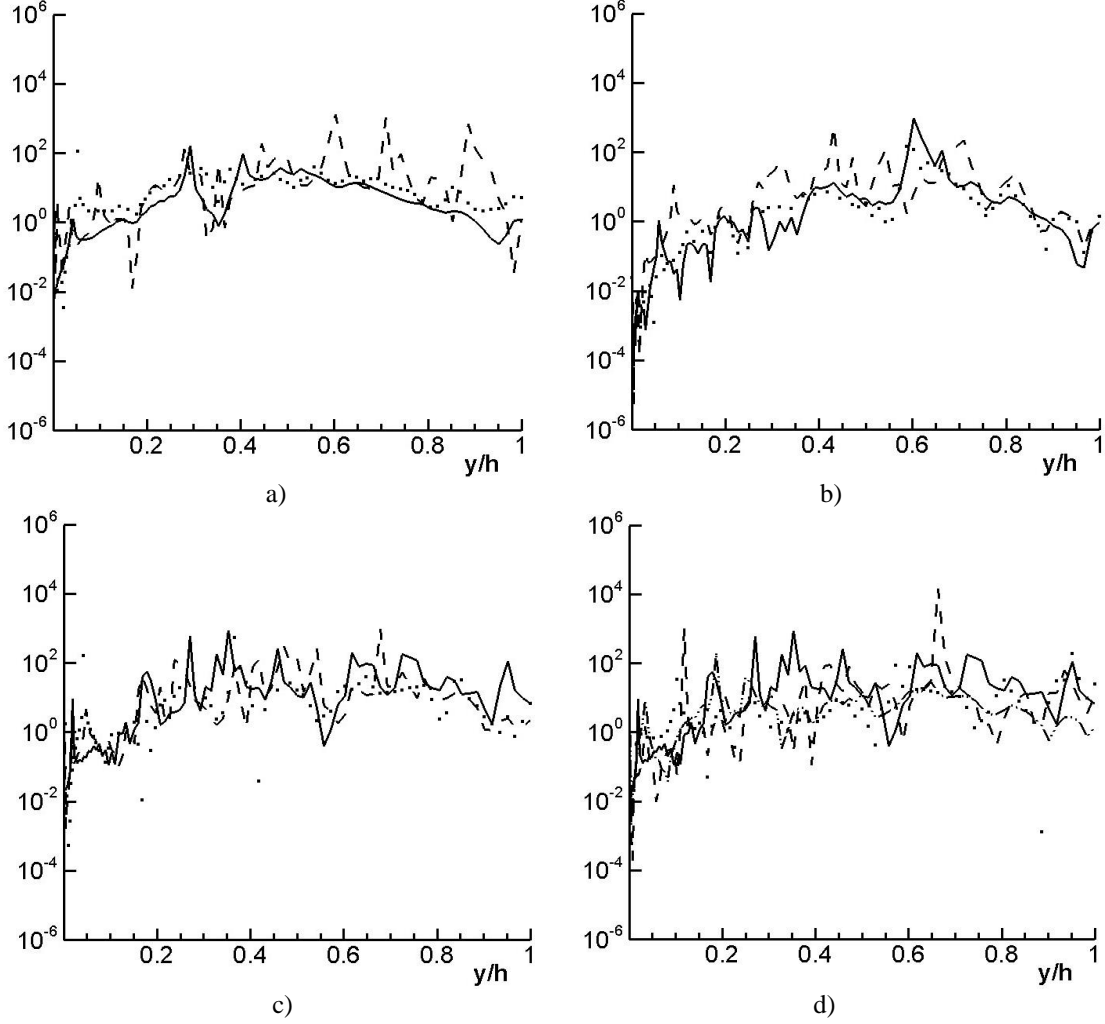


Fig. 19. Ratio of the balance errors to the molecular diffusion terms $|Err|'' = |Err / D^M|$ in the DNS⁹ budgets of velocity moments of different orders in the channel flow at $Re_\tau = 392$: a) $|Err_{yy}|''$, $|Err_{yyy}|''$, $|Err_{yyyy}|''$, b) $|Err_{xx}|''$, $|Err_{xxx}|''$, $|Err_{xxxx}|''$, c), $|Err_{xy}|''$, $|Err_{xyy}|''$, $|Err_{xyyy}|''$ and d) $|Err_{yx}|''$, $|Err_{xyx}|''$, $|Err_{xyxy}|''$, and $|Err_{xyxy}|''$. Notations: — errors in the Reynolds stresses budgets, - - - errors in the 3rd-order velocity moment budgets, ••• errors in the 4th-order velocity moment budgets except for $|Err_{xyxy}|''$, - · - · errors in the 4th-order velocity moment budget for $|Err_{xyxy}|''$.